

# Photoionization Models of NGC 346

Mónica Relaño<sup>1,2</sup>

Manuel Peimbert<sup>3</sup>

and

John Beckman<sup>1,4</sup>

## ABSTRACT

We present spherically symmetric and plane parallel photoionization models of NGC 346, an H II region in the Small Magellanic Cloud. The models are based on CLOUDY and on the observations of Peimbert, Peimbert, & Ruiz (2000). We find that approximately 45% of the H ionization photons escape from the H II region providing an important ionizing source for the low density interstellar medium of the SMC. The predicted  $I(4363)/I(5007)$  value is smaller than that observed, probably implying that there is an additional source of energy not taken into account by the models. From the ionization structure of the best model and the observed line intensities we determine the abundances of N, Ne, S, Ar, and Fe relative to O.

*Subject headings:* galaxies: abundances—galaxies: individual (SMC)—galaxies: ISM—H II regions—ISM: abundances

## 1. Introduction

NGC 346 is the most luminous H II region of the SMC, its H $\alpha$  luminosity places it on the boundary between normal and giant extragalactic H II regions. We have produced photoionization models of this object for the following reasons: a) to find if NGC 346 is density bounded or ionization bounded, b) to determine its chemical composition, and c)

---

<sup>1</sup>Instituto de Astrofísica de Canarias.

<sup>2</sup>Visiting Astronomer, Instituto de Astronomía, Universidad Nacional Autónoma de México.

<sup>3</sup>Instituto de Astronomía, Universidad Nacional Autónoma de México.

<sup>4</sup>Consejo Superior de Investigaciones Científicas.

to study the energy budget of the region. The photoionization models have been computed with CLOUDY 94 (Ferland 1996; Ferland et al. 1998).

The photoionization models computed in this paper present two advantages relative to similar models of extragalactic H II regions available in the literature: a) there are excellent line intensity observations available for this H II region (Peimbert, et al. 2000, hereinafter Paper I) ; b) the spectral types of most of the ionizing stars are known which permits us to adopt a representative ionizing flux. Most photoionization models in the literature are based on three assumptions: an IMF, an analytical fit to the adopted IMF, and a star formation history, these three assumptions introduce significant uncertainties in the ionizing flux (e.g., Cerviño, Luridiana, & Castander 2000).

## 2. Stellar Content and Photoionization Spectrum

We estimate directly the photoionization spectrum that will be used for the models based on the spectral classification of the blue stars presented by Massey, Parker, & Garmany (1989).

The ionized region of NGC 346 has a diameter of about  $420''$  and from the figures and coordinates presented by Massey et al. (1989) and Ye, Turtle, & Kennicutt (1991) we find that there are 58 blue stars with a visual apparent magnitude  $V < 15.6$  inside the ionized boundaries of NGC 346. The blue stars fainter than  $V = 15.6$  are expected to be of spectral type O9 or later and do not contribute appreciably to the photoionization spectrum.

Of the 58 stars considered by us 33 have pre-assigned spectral types and 25 do not. We have counted binary systems as single stars with the exception of HD 5980 where we consider independently the two main components (the system might have a third component).

We have assigned spectral types for the other 25 objects based on their  $V$  magnitudes and assuming that they are on the main sequence, these are the objects in parentheses presented in Table 1.

To derive the ionizing flux for all the stars in Table 1, with the exception of HD 5980, we have adopted the parameters presented by Vacca, Garmany, & Shull (1996).

For HD 5980 we have taken the stellar parameters derived by Schweickhardt & Schmutz(1999) where they have assumed that the luminosity of each component has remained constant during the 1987-1999 period, but varying the temperature and radius of component A. For the temperature of component A we have adopted the value it had at the end of 1990, the time of the observations that we are trying to match with the models. At this temperature the

stellar radius had the value of  $21.4 R_{\odot}$ .

The total ionizing flux is  $40.08 \times 10^{39} \text{ erg s}^{-1}$  (see Table 1). The ionizing fluxes of the objects without spectral types are presented in parentheses in Table 1; their combined flux amounts to  $8.80 \times 10^{39} \text{ erg s}^{-1}$ , 21.9% of the total value, which is a significant but relatively small fraction.

We estimate errors of 0.2 dex, 0.2 dex and 0.08 dex for the flux of HD 5980, the total flux of the stars in parentheses, and the total flux of all the other stars with known spectral types, respectively; consequently we have adopted an error of 0.08 dex for the total ionizing flux.

From the ionizing flux and the effective temperature for each star presented in Table 1 we have built three different photoionization spectra by adopting : *a*) blackbodies for all the stars, *b*) a set of stellar models for  $Z_* = Z_{\odot}$ , and *c*) a set of stellar models for  $Z_* = 0.2 Z_{\odot}$ . These three ionization spectra were chosen to estimate how sensitive are the properties of the models to changes in the adopted radiation field and consequently how general or robust are the results obtained from the models. The low metallicity set is based on the gaseous abundances for NGC 346 derived in Paper I and assumes that 20% of the heavy elements are trapped by dust inside the H II region (Esteban et al. 1998).

For the models with  $Z_* = Z_{\odot}$ , we chose: Mihalas (1972) atmospheres for the O3V star and for 5980A, Kurucz (1991) atmospheres for the stars of Luminosity Class I, and Schaerer & de Koter (1997) for the rest of the stars in Table 1. The models with  $Z_* = 0.2 Z_{\odot}$  are obtained using the library of stellar spectra built by Lejeune, Cuisinier, & Buser (1997); this library is based on three sets of atmosphere models and covers a wide range of physical stellar parameters. The three different ionizing continuum spectra used for the models are illustrated in Figure 1. The model sets are named as followed; series of models B, for blackbody spectra, series of models S for stellar models with  $Z_* = Z_{\odot}$  and series of models L for stellar spectra from Lejeune, Cuisinier, & Buser (1997).

Based on the models just described and assuming that all the ionizing photons are trapped by the nebula, the total ionizing flux (that is the same for all the models) implies an H $\alpha$  flux,  $L(\text{H}\alpha)$  in  $\text{erg s}^{-1}$ , of 39.216 dex for the model with  $Z_* = Z_{\odot}$ , 39.237 dex for the model with  $Z_* = 0.2 Z_{\odot}$ , and 39.25 dex assuming a blackbody spectrum. The small differences in the H $\alpha$  flux are due to the difference in the number of ionizing photons, which for a given ionizing flux does depend on the shape of the spectrum.

On the other hand, from the observed flux of  $1.55 \times 10^{-9} \text{ erg s}^{-1} \text{ cm}^{-2}$  (Kennicutt & Hodge 1996), an interstellar absorption correction,  $C(\text{H}\alpha)$ , of 0.10 dex (Paper I), and a distance to the SMC of 64 kpc (Reid 1999), we obtain a total emitted H $\alpha$  flux of  $38.98 \pm$

0.06 dex ( $\text{erg s}^{-1}$ ). Where the error is due to the combination of 0.04 dex, 0.02 dex, 0.01 dex errors in the observed flux, the adopted distance and  $C(\text{H}\alpha)$ , respectively.

The difference between the  $\text{H}\alpha$  flux predicted from the ionizing stellar radiation and the  $\text{H}\alpha$  flux derived from observations amounts to  $0.24 \pm 0.10$  dex,  $0.26 \pm 0.10$  dex and  $0.27 \pm 0.10$  dex for the models with  $Z_* = Z_\odot$ ,  $Z_* = 0.2 Z_\odot$  and for a blackbody spectrum respectively. These values imply that about  $45 \pm 15\%$  of the ionizing photons escape from NGC 346, and that the region is density bounded. Moreover, this result is in excellent agreement with the models to ionize the diffuse interstellar medium proposed by Zurita, Rozas, & Beckman (2000), and with the results of Oey & Kennicutt (1997), who find that many H II regions in the Large Magallanic Cloud are density bounded. This problem is discussed further in section 3.6.

The result that 45% of the photons escape is independent of the electron density distribution, but it does not necessarily imply that the H II region is density bounded in all directions, it is also possible to have a region which is density bounded in some directions and ionization bounded in others, these types of models require density distributions that are not radially symmetric, the simplest models that study this effect are those with a "covering factor", where in some directions all the photons escape and in others all the photons are trapped. We have assumed for the spherical models a constant density distribution or a density distribution that is spherically symmetric, therefore by density bounded we mean that photons escape in all directions. It is beyond the scope of this paper to model other types of density distributions.

## 2.1. Initial Mass Function

It is important to compare our ionizing flux distribution with that derived from a Salpeter IMF, for this purpose we will estimate the IMF of the massive stars responsible of most of the ionization.

In Figure 2 we present the IMF derived from Table 1 under the following assumptions: a) the main sequence stellar masses have been adopted as the initial masses, b) the mass of stars that are not in the main sequence has been adopted as their main sequence mass, c) for each star instead of an exact mass value we have adopted a uniform continuous distribution given by the central value  $\pm 0.02$  dex, d) we have fixed the lower mass limit of the last bin at  $51 M_\odot$ , which implies that this bin includes only half a star, e) the width of the bins corresponds to 0.08 dex, f) to derive the slope of the IMF we only considered the central four bins, we did not include the last bin because the IMF is truncated at the high mass end which

is inside this bin. We did not include the bin at the low mass end due to incompleteness, moreover the fraction of the ionizing flux due to the stars in this bin is negligible.

The fit to the central four bins defined in Figure 2 is given by

$$\log[N/\Delta \log m] = 7.675 - (3.71 \pm 0.4) \log m \quad (1)$$

this equation and point d) of the previous paragraph implies that the upper mass cutoff is equal to  $54.1 M_{\odot}$ . The slope given by equation (1) is considerably steeper than -2.35, the Salpeter slope, and indicates that for NGC 346 the use of the Salpeter slope to represent the ionizing flux is not adequate.

There are two other determinations of the IMF for the SMC. Massey et al. (1989) obtain  $-2.9 \pm 0.3$  in the  $9 M_{\odot}$  to  $85 M_{\odot}$  mass range for NGC 346 and Humphreys and McElroy (1984) obtain -3.1 in the  $15 M_{\odot}$  to  $100 M_{\odot}$  mass range for the SMC. From the data of Humphreys and McElroy we obtain a slope of -3.7 for the  $25 M_{\odot}$  to  $100 M_{\odot}$  mass range, in excellent agreement with the slope derived by us.

Our IMF for NGC 346 implies that for extragalactic H II regions with an H $\alpha$  flux similar or smaller than that of NGC 346 it is difficult to determine  $M_{\text{up}}$ , and that the slope, at least for masses higher than  $24 M_{\odot}$ , might be steeper than the slope given by a Salpeter IMF.

To determine the ionizing flux for an extragalactic H II region based on an analytical function we need to know: a) the slope of the IMF, b) the  $M_{\text{up}}$ , c) the fraction of ionizing photons that are trapped by the H II region, and d) the star formation history of the burst that produced the H II region. As discussed above these four problems indicate that for NGC 346 it is considerably better to use the ionizing flux determined from the individual stars than to derive the ionizing flux based on an analytical approximation to the IMF.

### 3. Photoionization Models

All the models discussed in this paper were computed with CLOUDY. For all models, with the exception of those with enhanced and depleted abundances (models L.5 and L.6), we adopted the following chemical composition (given in  $\log N(X)/N(\text{H}) + 12$ ): He = 10.90, C = 7.39, N = 6.51, O = 8.11, Ne = 7.30, Mg = 5.98, Si = 6.37, S = 6.59, Cl = 4.80, Ar = 5.82, and Fe = 5.58. Where the He, N, O, Ne, S and Ar are the gaseous abundances derived in Paper I, C/O is the value derived by Garnett et al. (1995) for the SMC, and Mg/O, Si/O and Fe/O come from the gaseous abundances derived by Esteban et al. (1998) for the Orion nebula.

As mentioned in section 2 we used three different sets of ionizing fluxes: atmospheres with  $Z_* = 0.2 Z_\odot$  (models L), atmospheres with  $Z_* = Z_\odot$  (models S), and blackbody radiation fields (models B). The reason to use these three sets of ionizing fluxes is to explore how general are the conclusions based on the L models. In Figure 1 we show the three integrated spectra used as the input ionization for the models.

To compare the observed values with the models computed with CLOUDY we used the radial integrations of the models that include the center and compared them with the average intensities of Regions 3 and 13 which are close to the center. We took the average of the two regions to reduce the observational errors and to obtain a more representative value of a line of sight towards the center of the object. All the models have an inner radius,  $r_0$ , of  $10^{16}$  cm, with the exception of models L.7 and B.3.

We also present in Tables 2 and 3 the line intensities of region A (that includes the average intensities of 13 regions) because the errors are smaller than those of the average intensities of regions 3 and 13 and to show that the differences between the two sets of line intensities are relatively small. For similar reasons we also present  $T_e(\text{rad})\text{K}$  and  $T_e(\text{vol})\text{K}$  the radial and the volume averaged temperatures weighted by  $N_e N(\text{O}^{++})$  obtained from the models, and  $T_e([\text{O III}])\text{K}$  the volume averaged temperature obtained from the  $I(4363)/I(5007)$  ratio. To compare the line intensities with those of regions 3 and 13, all the line intensities have been radial averaged. The main reason for selecting the line ratios presented in Tables 2, 3 and 4 is that they are very sensitive to changes in the input parameters for the models, thus allowing us to obtain a robust model for the observed region. In particular the  $[\text{O II}]/[\text{O III}]$  ratios are very sensitive to the degree of ionization, and the  $[\text{O II}]$ ,  $[\text{S II}]$ , and  $[\text{O I}]$  to  $\text{H}\beta$  line ratios give us information on the behaviour of the low degree of ionization regions of the nebula. All these line ratios are also sensitive to the density distribution adopted.

In sections 3.1 to 3.5 we discuss density bounded models in all directions in agreement with the results presented in section 2. In section 3.6 we discuss two ionization bounded models which provide independent support for the view that NGC 346 is a density bounded nebula.

### 3.1. Constant density models

The simplest models that can be computed are spherical with constant density (models L.1, S.1, and B.1). The density is given by the root mean square density,  $N_e(\text{rms})$ , and takes the value  $9.00 \text{ cm}^{-3}$ . This value was derived from the  $\text{H}\alpha$  flux from Kennicutt & Hodge (1986), a  $C(\text{H}\alpha)$  of 0.10 dex (Paper I), a distance to the SMC of 64 kpc (Reid 1999, and

references therein), and a radius of  $210''$ .

Using these models we find that most of the predicted line ratios differ considerably from the observed ones. In particular the lines of low degree of ionization, such as those of O II and S II, are very faint (see Table 2).

By looking at the [O II] and [O III] line intensities it can be seen that the degree of ionization increases in the B.1, A.1, S.1 sequence this result permits us to estimate the differences in the models due to the ionization field adopted.

### 3.2. Models with filling factor different from 1.0

Considering the filamentary aspect of NGC 346 (e.g. Ye et al. 1991), the densities derived in Paper I, and the weakness of the lines with low degree of ionization, we decided to compute a model with a filling factor different from 1, and a constant  $N_e(\text{local})$ .

The filling factor can be estimated by means of the relation:

$$N_e^2(\text{rms}) = \epsilon N_e^2(\text{local}), \quad (2)$$

where  $N_e(\text{rms})$  is the root mean square electron density, and  $N_e(\text{local})$  is the electron density determined through a forbidden-line ratio or from the He I lines based on the maximum likelihood method (see Paper I). The He I lines originate in the (He II) zone, therefore the density derived from them is called the (He II) density.

We computed models of the L series with different filling factors and the best fit to the observed O II/H $\beta$ , O III/H $\beta$ , and O III/O II ratios is provided by model L.4 with an  $N_e(\text{local})$  of  $80 \text{ cm}^{-3}$  and a filling factor  $\epsilon$  of 0.0127. By comparing the line ratios predicted by model L.4 with observations (see Table 2) we find a much better fit than that provided by model L.1. Also in Table 2 we present models L.2 and L.3 to show the sensitivity of the fit to the adopted density (or filling factor).

We also computed models of the S series with different filling factors and present them in Table 3. Model S.2, which has the same density and filling factor as model L.2, provides a considerably better fit to the observations than the S.1 model, in agreement with the result obtained with the L series. As with the case of the L.1 and S.1 models, the S.2 model shows a higher degree of ionization than the L.2 model. By increasing the density it is possible to obtain a better O II/H $\beta$  fit with a model of the S series, but the fit of the O III/O II and the O III/H $\beta$  ratios becomes poorer.

Models with  $0.005 < \epsilon < 0.02$  provide a much better fit to the observations than models

with  $\epsilon = 1.00$  (see Tables 2 and 3).

### 3.3. Decreasing density models

We have two determinations of  $N_e(\text{local})$ ,  $N_e(\text{He II}) = 143 \pm 36 \text{ cm}^{-3}$  and  $N_e(\text{S II}) = 50 \pm 15 \text{ cm}^{-3}$ . Since the sulfur emission originates in the outer parts and the helium emission all over the H II region, we decided to compute two models with higher density in the center and lower in the outer regions.

Model L.7 has the following decreasing density law:

$$N(r) = N_0 \left( \frac{r}{r_0} \right)^{-\alpha}, \quad (3)$$

where  $r_0$  and  $N_0$  are, respectively, the inner radius and the density at the inner radius. We choose a density law with an exponent  $\alpha=0.315$ , which gives a value of  $180 \text{ cm}^{-3}$  at  $r_0 = 10^{19} \text{ cm}$  and a value of  $70 \text{ cm}^{-3}$  at the boundary ( $r = 2.0 \times 10^{20} \text{ cm}$ ). From the observational constraint in the  $\text{H}\alpha$  flux we obtained that  $\epsilon = 0.013$ .

Model B.2 is made of two concentric spherical shells with  $N_e(\text{local})$  equal to 140 and  $50 \text{ cm}^{-3}$  respectively and the following radial intervals:  $10^{16}$  to  $10^{20}$  and  $10^{20}$  to  $2.0 \times 10^{20} \text{ cm}$  respectively.

Models L.7 and B.2 provide a better fit to the observations than models L.1 and B.1, but do not provide a significantly better fit than L.4, the main reference model.

### 3.4. Models with different chemical composition

Models L.5 and L.6 were computed with 0.1 dex higher and 0.1 dex lower heavy element abundances than model L.4. The differences in the O/H value are about  $2\sigma$  higher for model L.5 and  $2\sigma$  lower for model L.6 than the values derived in Paper I.

Model L.5 produces a modest increase in respect to model L.4 in the  $I(3727+5007)/I(H\beta)$  value without reaching the observed value. Alternatively the difference between the predicted and the observed  $I(4363)/I(5007)$  value becomes larger than in model L.4.

Model L.6 produces a higher  $I(4363)/I(5007)$  value than model L.4 without reaching the observed value. Alternatively the difference between the observed and predicted  $I(3727+5007)/I(H\beta)$  value becomes larger than in model L.4.



### 3.5. Plane-parallel models

We decided to study a completely different geometric arrangement to see if it was possible to get a better agreement between models and observations. In addition to one dimensional models with spherical symmetry, it is possible to compute one dimensional plane parallel models. For these models we have adopted five observational restrictions associated with the geometry: a) the distance to the object, b) the subtended solid angle, c) the observed  $H\alpha$  flux, d) an  $N_e(\text{local})=100 \text{ cm}^{-3}$ , and e) the incident flux per unit area in the direction of the line of sight, that we assume to be constant all over the face of the nebula. The incident flux per unit area is given by the ionizing stellar flux divided by the area perpendicular to the line of sight.

The line intensities predicted by one of our plane parallel models (B.3) are presented in Table 3. The model has an area perpendicular to the line of sight of  $1.26 \times 10^{41} \text{ cm}^2$  and a length in the direction of the line of sight of  $0.9 \times 10^{20} \text{ cm}$ , which implies an  $\epsilon$  of 0.0216. The model provides a poorer fit than the spherical models because it shows a considerably lower degree of ionization than the observations.

Other geometries require two or three dimensional photoionization codes and are beyond the scope of this paper.

### 3.6. Ionization bounded

To explore further the possibility that NGC 346 is a density bounded H II region, we have studied three line ratios involving lines with low degree of ionization:  $I(\lambda 6300)/I(H\beta)$ ,  $I(\lambda 6717)/I(H\beta)$ , and  $I(\lambda 3727)/I(H\beta)$ . These ratios are stronger in the outer zones of an ionization bounded H II region than in the outer zones of a density bounded H II region. In Table 4 we show these line ratios for each model as well as the observational values from Paper I. For  $I(\lambda 6300)/I(H\beta)$ , all the density bounded models give a value of the line ratio in agreement with the observational limit, and models L.2 to L.6, B.2, and S.2 show good agreement with the other two lines.

In Table 4 we present these three line ratios for two ionization bounded models, IL.4 and IS.2. These models are similar to the density bounded models L.4 and S.2 the only difference is that the intensity of the ionizing flux is 45% smaller than in the density bounded models so that all the ionizing photons are trapped by the nebula. For the IS.2 model the three line ratios are stronger than observed, while for the IL.4 model the predicted  $I(\lambda 6300)/I(H\beta)$  value is smaller than the upper limit while the other two line ratios are stronger than observed. To reach agreement between ionization bounded models and the

observations it is necessary to reduce  $N_e(\text{local})$  (and to increase the filling factor accordingly) entering into conflict with the observed  $N_e(\text{He II}) = 143 \pm 36 \text{ cm}^{-3}$  and  $N_e(\text{S II}) = 50 \pm 15 \text{ cm}^{-3}$  values. Of the line ratios presented in Table 4 the best discriminant between the density bounded and the ionization bounded models is the  $I(\lambda 6300)/I(H\beta)$  value, therefore it is important to obtain a determination of this line ratio and not only an upper limit. The previous discussion supports the result that NGC 346 is a density bounded nebula.

Models for NGC 346 with a covering factor of 0.55 will produce intermediate ionization structures to those provided by density bounded and ionization bounded models. From the discussion of the previous paragraph it follows that these models will produce better fits to the lines of low degree of ionization than the ionization bounded models but poorer fits than the density bounded models.

#### 4. Ionization Correction Factors and Abundances

For most of the elements we observe only one or two stages of ionization, therefore to obtain the total abundances relative to H we need to determine the fraction of a given element present in the unobserved stages of ionization. Therefore to obtain the total abundances we have made use of the following equations:

$$\frac{N(\text{O})}{N(\text{H})} = \frac{N(\text{O}^+) + N(\text{O}^{++})}{N(\text{H}^+)}, \quad (4)$$

$$\frac{N(\text{N})}{N(\text{H})} = ICF(\text{N}) N(\text{N}^+)/N(\text{H}^+), \quad (5)$$

$$\frac{N(\text{Ne})}{N(\text{H})} = ICF(\text{Ne}) N(\text{Ne}^{++})/N(\text{H}^+), \quad (6)$$

$$\frac{N(\text{S})}{N(\text{H})} = ICF(\text{S}) N(\text{S}^+ + \text{S}^{++})/N(\text{H}^+), \quad (7)$$

$$\frac{N(\text{Ar})}{N(\text{H})} = ICF(\text{Ar}) \frac{N(\text{Ar}^{++}) + N(\text{Ar}^{3+})}{N(\text{H}^+)}, \quad (8)$$

$$\frac{N(\text{Fe})}{N(\text{H})} = ICF(\text{Fe}) N(\text{Fe}^{++})/N(\text{H}^+); \quad (9)$$

where the ionization correction factors,  $ICF'$ s, were estimated from the models presented in this paper, see Table 5, and the ionic abundance ratios were taken from Paper I. To obtain the  $N(\text{Fe}^{++})/N(\text{H}^+)$  value we made use of the observed intensity of  $\lambda 4568$  in region A and its predicted intensity by the models. The total abundances are presented in Table 6.

The He/H value is given by (e.g. Sauer & Jedamzik 2001; Peimbert 2001 and references therein):

$$\begin{aligned} \frac{N(\text{He})}{N(\text{H})} &= \frac{\int N_e N(\text{He}^0) dV + \int N_e N(\text{He}^+) dV + \int N_e N(\text{He}^{++}) dV}{\int N_e N(\text{H}^0) dV + \int N_e N(\text{H}^+) dV}, \\ &= ICF(\text{He}) \frac{\int N_e N(\text{He}^+) dV + \int N_e N(\text{He}^{++}) dV}{\int N_e N(\text{H}^+) dV}, \end{aligned} \quad (10)$$

where  $ICF(\text{He})$  is the helium ionization correction factor. To determine a very accurate He/H ratio a very precise value of  $ICF(\text{He})$  is needed. As expected for our density bounded models it is found that  $ICF(\text{He}) = 1.000$ , because there is no transition zone from ionized to neutral He and H regions.

## 5. Discussion and Conclusions

We have presented a set of photoionization models for NGC 346. The advantage of these models relative to those models present in the literature of giant extragalactic H II regions is that we know the spectra of most of the ionizing stars and the absolute V magnitude for all of them, therefore we did not have to assume the IMF, the age of the cluster, the star formation rate, nor the fraction of ionizing photons that are trapped by the nebula.

The models were computed with different geometries, different density distributions, different chemical compositions and different radiation fields. We did not compute models composed via a superposition of separate individual Strömgen spheres because a considerable amount of the ionizing flux escaped from the nebula implying that the Strömgen spheres produced by each star overlap, and that the single H II region model is a good approximation.

By comparing the models with the observed line intensity ratios we obtain the following results:

1) Spherical models with constant density, with  $\epsilon = 1.00$  (models L.1, S.1, and B.1), attain a high degree of ionization that is not observed. Moreover, these models have an  $N_e(\text{rms}) = 9.00 \text{ cm}^{-3}$ , this density is smaller than those derived from the [S II] and He I lines (see Paper I).

2) Spherical models (L.4, L.7, S.2 and B.2) can reproduce the observed degree of ionization and show good agreement with the [S II] and He II densities.

3) Models L.7 and B.2 include more realistic density distributions, but their predictions are not very different to those of models L.4 and S.2.

4) The  $I(\text{He II}, 4686)/I(\text{H}\beta)$  ratio is very small and is very sensitive to small changes in the radiation field and the geometry of the H II region. Model L.1 has the same geometry as models S.1 and B.1 but shows a difference of about an order of magnitude in the  $I(\text{He II}, 4686)/I(\text{H}\beta)$  ratio. The differences are due to the three radiation fields used which vary in the fraction of photons with an energy higher than four Rydbergs, while in model B.1 we use a blackbody spectrum as an ionizing source, in models L.1 and S.1 we use two different sets of stellar atmospheres (see Figure 1).

Models L.2 to L.6 have similar  $I(\text{He II}, 4686)/I(\text{H}\beta)$  ratios while model L.7 shows a ratio that is about two orders of magnitude fainter than the other L models. All the models of the L series have the same radiation field, in this case the difference is due to the geometry, the L.7 model has an inner hole of  $10^{19}$  cm while the other L models have an inner hole of  $10^{16}$  cm, the different geometry dilutes the radiation field in the inner regions of the nebula causing the drop in the helium ionization degree. A similar drop in the ionization degree, due to geometrical effects, is present in the plane parallel model B.3, which shows an  $I(\text{He II}, 4686)/I(\text{H}\beta)$  ratio two orders of magnitude fainter than the spherical models B.1 and B.2.

5) Plane parallel models present a considerably lower degree of ionization than is observed in NGC 346. For example they underestimate the  $I([\text{Ar IV}], 4740)/I([\text{Ar III}], 7135)$  and the  $I([\text{O III}], 5007)/I([\text{O II}], 3727)$  ratios. On the other hand spherical models (like L.4, L.7, S.2 and B.2) present line ratios in good agreement with the observations.

6) None of the models are able to reproduce the observed  $I(3727 + 5007)/I(\text{H}\beta)$  ratio nor the  $I(5007)/I(4363)$  ratio. This is a crucial result which implies that photoionization models predict lower temperatures than those observed. This result probably implies that there are additional heating sources not considered by the photoionization models. Similar results were obtained by Stasińska & Schaerer (1999) for I Zw 18, Luridiana, Peimbert, & Leitherer (1999) for NGC 2363, and Luridiana & Peimbert (2001) for NGC 5461.

7) The total abundances of N, Ne, S, Ar, and Fe were obtained from the *ICF's* predicted by model L.4. By comparing the empirical *ICF's* in Paper I with those derived from model L.4 we find excellent agreement for Ne and Ar, good agreement for S, and only a fair agreement for N. Based on empirical methods and on photoionization models it has been found that the  $\text{O}^+$  zone coincides with the  $\text{N}^+$  zone and consequently that the N/O ratio is equal to the  $\text{N}^+/\text{O}^+$  ratio (e. g. Peimbert & Costero 1969; Garnett 1990; Mathis & Rosa 1991; Stasińska & Schaerer 1997, Paper I); alternatively the N abundance derived from the NGC 346 CLOUDY models differs by about a factor of two from that derived from the  $\text{N}^+/\text{O}^+$

ratio (see Table 6), Stasińska & Schaerer (1997) have studied this discrepancy and conclude that it is due to the different ionizing spectra used by different authors.

From a detailed comparison between stellar ionizing photon input and the observed  $H\alpha$  flux we infer that some 45% of the photons produced by the ionizing stars escape from NGC 346. This result is independent of the geometry and of the density distribution of the nebula, and implies that this object must be a major source of ionizing flux for the surrounding diffuse interstellar medium. The ionization bounded models we have tried fail completely to match the intensities of lines with a low degree of ionization, but these can be matched using density bounded models, which supports strongly the conclusion that NGC 346 is density bounded.

It is a pleasure to acknowledge fruitful discussions with Valentina Luridiana and Antonio Peimbert. We are also very grateful to Grazyna Stasińska for a thorough reading of a previous version of this paper and many excellent suggestions. M.R. acknowledges financial help from DGES grant PB97-0219 which facilitated her stay at the UNAM during a major phase of this study.

## REFERENCES

- Cerviño, M., Luridiana, V., & Castander, F.J. 2000, *A&A*, 360, L5
- Esteban, C., Peimbert, M., Torres-Peimbert, S., & Escalante, V. 1998, *MNRAS*, 295, 401
- Esteban, C., Peimbert, M., Torres-Peimbert, S., & García-Rojas, J. 1999, *RevMexAA*, 35, 85
- Ferland, G. J. 1996, *Hazy, a Brief Introduction to CLOUDY 90* (Univ. Kentucky Dept. Phys. Astron. Internal Rep.)
- Ferland, G. J., Korista, K. T., Verner, D. A., Ferguson, J. W., Kingdon, J. B., & Verner, E. M. 1998, *PASP*, 110, 761
- Garnett, D. R. 1990, *ApJ*, 363, 142
- Garnett, D. R., Skillman, E. D., Dufour, R. J., Peimbert, M., Torres-Peimbert, S., Terlevich, R. J., Terlevich, E., & Shields, G. A., 1995, *ApJ*, 443, 64
- Grevesse, N. & Sauval, A. J. 1998, *Space Sci. Rev.*, 85, 161
- Humphreys, R. M., & McElroy, D. B. 1984, *ApJ*, 284, 565

- Kennicutt, R. C., Jr., & Hodge, P. W. 1986, ApJ, 306, 130
- Koenigsberger, G., Auer, L. H., Georgiev, L., & Guinan, E. 1998, ApJ, 496, 934
- Kurucz, R. L., 1991, in Proceedings of the Workshop on Precision Photometry: Astrophysics of the Galaxy, A. C. Davis Philip, A. R. Upgren, & K. A. James (Davis, Schenectady), p 27
- Lejeune, Th., Cuisinier, F., & Buser, R. 1997, 125, 229
- Luridiana, V., & Peimbert, M. 2001, ApJ, 553, 663
- Luridiana, V., Peimbert, M., & Leitherer, C. 1999, ApJ, 527, 110
- Massey, P., Parker, J. W., & Garmany, C. D. 1989, AJ, 98, 1305
- Mathis, J. S., & Rosa, M. R. 1991, A&A, 245, 625
- Mihalas, D. 1972, Non-LTE Model Atmosphere for B&O Stars (NCAR-TN/-STR-76; Denver:NCAR)
- Oey, M. S., & Kennicutt, R. C., Jr. 1997, MNRAS, 291, 827
- Peimbert, M. *Revista Mexicana de Astronomía y Astrofísica, Serie de Conferencias*, in press (astro-ph/0106063), 2001.
- Peimbert, M. & Costero, R. 1969, Bol. Obs. Tonantzintla y Tacubaya, 5, 3
- Peimbert, M., Peimbert, A., & Ruiz, M.T. 2000, ApJ, 541, 688, Paper I
- Peimbert, M., Torres-Peimbert, S., & Ruiz, M.T. 1992, RevMexAA, 24, 155
- Reid, I. N. 1999, ARA&A, 37, 191
- Sauer, D., & Jedamzik, K. 2001, A&A, submitted (astro-ph/0104392)
- Schaerer, D., & de Koter, A. 1997, A&A, 322, 598
- Schweickhardt, J., & Schmutz, W. 1999, in IAU Symp. 193, Wolf-Rayet Phenomena in Massive Stars and Starburst Galaxies, ed. K. A. van der Hucht, G. Koenigsberger & P. R. J. Enns (San Francisco: ASP), 101
- Stasińska, G., & Schaerer, D. 1997, A&A, 322, 615
- Stasińska, G., & Schaerer, D. 1999, A&A, 351, 72

Vacca, W.D., Garmany, C. D., & Shull, J. M. 1996, *ApJ*, 460, 914

Ye, T., Turtle, A.J., & Kennicutt, R. C., Jr. 1991, *MNRAS*, 249, 722

Zurita, A., Rozas, M., & Beckman, J. E. 2000, *A&A*, 363, 9

Table 1. Spectral Types, Temperatures, Mass, and Ionizing Fluxes

Spectral Type	$T$ (K)	$M$ ( $M_{\odot}$ )	Number of stars	Ionizing Flux ( $10^{39}\text{erg s}^{-1}$ )
O3V	51230 <sup>a</sup>	51.3 <sup>a</sup>	1	2.02
O4V	48670 <sup>a</sup>	44.2 <sup>a</sup>	1	1.43
O5.5V	44840 <sup>a</sup>	35.5 <sup>a</sup>	3 (1)	2.46 (0.82)
O6V	43560 <sup>a</sup>	33.1 <sup>a</sup>	3 (1)	2.07 (0.69)
O6.5V	42280 <sup>a</sup>	30.8 <sup>a</sup>	2 (1)	1.14 (0.57)
O7V	41010 <sup>a</sup>	28.8 <sup>a</sup>	3 (2)	1.40 (0.94)
O7.5V	39730 <sup>a</sup>	26.9 <sup>a</sup>	2 (2)	0.76 (0.76)
O8V	38450 <sup>a</sup>	25.1 <sup>a</sup>	6 (7)	1.88 (2.20)
O8.5V	37170 <sup>a</sup>	23.6 <sup>a</sup>	1 (11)	0.26 (2.82)
O9V	35900 <sup>a</sup>	22.1 <sup>a</sup>	2	0.43
O9.5V	34620 <sup>a</sup>	20.8 <sup>a</sup>	5	0.86
O5.5I	43210 <sup>a</sup>	45.4 <sup>a</sup>	1	4.93
O7I	38720 <sup>a</sup>	37.4 <sup>a</sup>	1	1.77
WN4(5980A)	52000 <sup>b</sup>	18.0 <sup>c</sup>	1	7.01
O7Ia(5980B)	31135 <sup>b</sup>	37.4 <sup>a</sup>	1	2.86
Total	...	...	33 (25)	31.28 (8.80)

<sup>a</sup>Vacca et al. (1996).

<sup>b</sup>Schweickhardt & Schmutz(1999).

<sup>c</sup>Koenigsberger et al. (1998)



Table 2. Photoionization models based on a set of atmospheres with  $Z_* = 0.2Z_\odot$

Line ratios <sup>a</sup>	Reg. A	Reg 3 and 13	Mod L.1	Mod L.2	Mod L.3	Mod L.4	Mod L.5	Mod L.6	Mod L.7
[O III] $I(\lambda 5007)/I(\lambda 3727)$	0.738	0.750	1.633	0.492	0.383	0.595	0.597	0.578	0.769
[S III] $I(\lambda 6312)/I(\lambda 6725)$	-0.857	-0.744	-0.004	-0.883	-0.974	-0.802	-0.847	-0.776	-0.659
[Ar IV] $I(\lambda 4740)/I(\lambda 7135)$	-1.111	-1.392	-0.614	-1.233	-1.292	-1.179	-1.214	-1.155	-1.136
[O III] $I(\lambda 4363)/I(\lambda 5007)$	-1.854	-1.915	-2.041	-2.015	-2.010	-2.021	-2.100	-1.951	-2.018
He II $I(\lambda 4686)/I(\lambda 4471)$	-1.155	-1.430	-0.905	-1.286	-1.337	-1.242	-1.243	-1.243	-3.209
[S II] $I(\lambda 6716)/I(\lambda 6731)$	0.144	0.142	0.152	0.116	0.106	0.124	0.124	0.123	0.123
[S II] $I(\lambda 4069 + 4076)/I(\lambda 6725)$	-1.115	-0.940	-1.104	-1.050	-1.038	-1.060	-1.086	-1.037	-1.060
[O III] $I(\lambda 5007)/I(H\beta)$	0.735	0.710	0.625	0.541	0.518	0.559	0.579	0.526	0.609
[O II] $I(\lambda 3727)/I(H\beta)$	-0.003	-0.040	-1.008	0.049	0.135	-0.036	-0.018	-0.052	-0.160
He II $I(\lambda 4686)/I(H\beta)$	-2.571	-2.844	-2.419	-2.804	-2.856	-2.759	-2.753	-2.766	-4.708
$L(H\alpha)$ (dex)	...	...	38.987	38.978	38.987	38.977	38.988	38.981	38.989
$N_e$ (rms)( $\text{cm}^{-3}$ )	...	...	9.00	9.00	9.00	9.00	9.00	9.00	9.00
radius ( $10^{20}$ cm)	...	...	2.00	2.01	2.01	2.01	2.00	2.04	2.02
$N_e$ (local)	...	...	9.00	100	130	80	80	80	...
$\epsilon$	...	...	1.00	0.0081	0.005	0.0127	0.0127	0.0127	0.013
[O] <sup>b</sup>	...	...	8.11	8.11	8.11	8.11	8.21	8.01	8.11
$T_e$ (rad)K	...	...	11200	11400	11500	11400	10700	12000	11400
$T_e$ (vol)K	...	...	10800	11200	11300	11100	10600	11700	11100
$T_e$ ([O III])K	13070	12430	10800	11300	11300	11200	10600	11800	11200

<sup>a</sup>Given by  $\log I(\lambda_1)/I(\lambda_2)$ .

<sup>b</sup>Gaseous abundances given by  $12 + \log N(\text{O})/N(\text{H})$ .

Table 3. Photoionization models based on other sets of stellar atmospheres

Line ratios <sup>a</sup>	Reg. A	Reg 3 and 13	Mod S.1 <sup>b</sup>	Mod S.2 <sup>b</sup>	Mod B.1 <sup>c</sup>	Mod B.2 <sup>c</sup>	Mod B.3 <sup>c</sup>
[O III] $I(\lambda 5007)/I(\lambda 3727)$	0.738	0.750	1.918	0.716	1.435	0.759	0.190
[S III] $I(\lambda 6312)/I(\lambda 6725)$	-0.857	-0.744	-0.065	-0.927	-0.054	-0.587	-0.882
[Ar IV] $I(\lambda 4740)/I(\lambda 7135)$	-1.111	-1.392	-0.346	-0.994	-0.812	-1.156	-2.581
[O III] $I(\lambda 4363)/I(\lambda 5007)$	-1.854	-1.915	-1.981	-1.976	-2.077	-2.039	-2.078
He II $I(\lambda 4686)/I(\lambda 4471)$	-1.155	-1.430	0.293	0.183	0.359	0.359	-1.916
[S II] $I(\lambda 6716)/I(\lambda 6731)$	0.144	0.142	0.150	0.117	0.152	0.112	0.116
[S II] $I(\lambda 4069 + 4076)/I(\lambda 6725)$	-1.115	-0.940	-1.080	-1.043	-1.125	-1.065	-1.065
[O III] $I(\lambda 5007)/I(H\beta)$	0.735	0.710	0.663	0.607	0.595	0.585	0.478
[O II] $I(\lambda 3727)/I(H\beta)$	-0.003	-0.040	-1.255	-0.109	-0.840	-0.174	0.288
He II $I(\lambda 4686)/I(H\beta)$	-2.571	-2.844	-1.255	-1.360	-1.132	-1.137	-3.338
$L(H\alpha)$ (dex)	...	...	38.981	38.973	38.975	38.989	38.993
$N_e$ (rms)( $\text{cm}^{-3}$ )	...	...	9.00	9.00	9.00	9.00	9.00
radius ( $10^{20}$ cm)	...	...	2.01	2.01	1.94	2.00	...
$R_1$ ( $10^{20}$ cm)	...	...	...	...	...	1.01	...
$N_e$ (local)	...	...	9.00	100	9.00	(140,50)	100
$\epsilon$	...	...	1.00	0.0081	1.00	0.0175	0.0216
[O] <sup>d</sup>	...	...	8.11	8.11	8.11	8.11	8.11
$T_e$ (rad)K	...	...	11700	11700	10800	11100	10900
$T_e$ (vol)K	...	...	11200	11400	10400	10800	10900
$T_e$ ([O III])K	13070	12430	11300	11500	10400	10800	11000

<sup>a</sup>In units of  $\log I(\lambda_1)/I(\lambda_2)$ .

<sup>b</sup> $Z_* = Z_\odot$

<sup>c</sup>Blackbody ionizing spectrum.

<sup>d</sup>Gaseous abundances given by  $12 + \log N(\text{O})/N(\text{H})$ .

Table 4. Line ratios of [O I], [S II], and [O II]

Models	$I(\lambda 6300)/I(H\beta)$	$I(\lambda 6717)/I(H\beta)$	$I(\lambda 3727)/I(H\beta)$
$Z_* = 0.2Z_\odot$			
L.1	-5.402	-2.244	-1.008
L.2	-3.155	-1.140	0.049
L.3	-2.953	-1.042	0.135
L.4	-3.340	-1.230	-0.036
L.5	-3.289	-1.279	-0.018
L.6	-3.362	-1.174	-0.052
L.7	-3.609	-1.327	-0.334
Blackbody Spectrum			
B.1	-5.277	-2.136	-0.840
B.2	-3.878	-1.433	-0.174
B.3	-3.328	-1.029	0.288
$Z_* = Z_\odot$			
S.1	-5.600	-2.297	-1.255
S.2	-3.219	-1.116	-0.109
IL.4 <sup>a</sup>	-2.270	-0.861	0.234
IS.2 <sup>a</sup>	-1.707	-0.844	0.193
Observations <sup>b</sup>	< -2.016	-1.284	-0.040

<sup>a</sup>Ionization bounded models, see text

<sup>b</sup>For Region A and from Paper I

Table 5. Ionization Correction Factors for Region A

Element	Paper I	This paper
N	5.62	11.22
Ne	1.23	1.29
S	1.98	1.29
Ar	1.21	1.22
Fe	...	8.00:

Table 6. Total Abundances<sup>a</sup>

Element	NGC 346 Paper I	NGC 346 This paper	Sun <sup>b</sup>	Orión <sup>c</sup>	M17 <sup>d</sup>
N	6.51	6.81	7.92	7.78	7.90
O <sup>e</sup>	8.15	8.15	8.83	8.72	8.87
Ne	7.30	7.32	8.08	7.89	8.02
S	6.59	6.40	7.33	7.17	7.31
Ar	5.82	5.82	6.40	6.49	6.60
Fe <sup>f</sup>	...	6.16	7.50	6.11	6.69

<sup>a</sup>In units of  $12 + \text{Log } N(\text{X})/N(\text{H})$ .

<sup>b</sup>Grevesse & Sauval (1998).

<sup>c</sup>Esteban et al. (1998).

<sup>d</sup>Peimbert, Torres-Peimbert, & Ruiz (1992); Esteban et al. (1999).

<sup>e</sup>Gas plus dust for the H II regions.

<sup>f</sup>Gaseous content only.

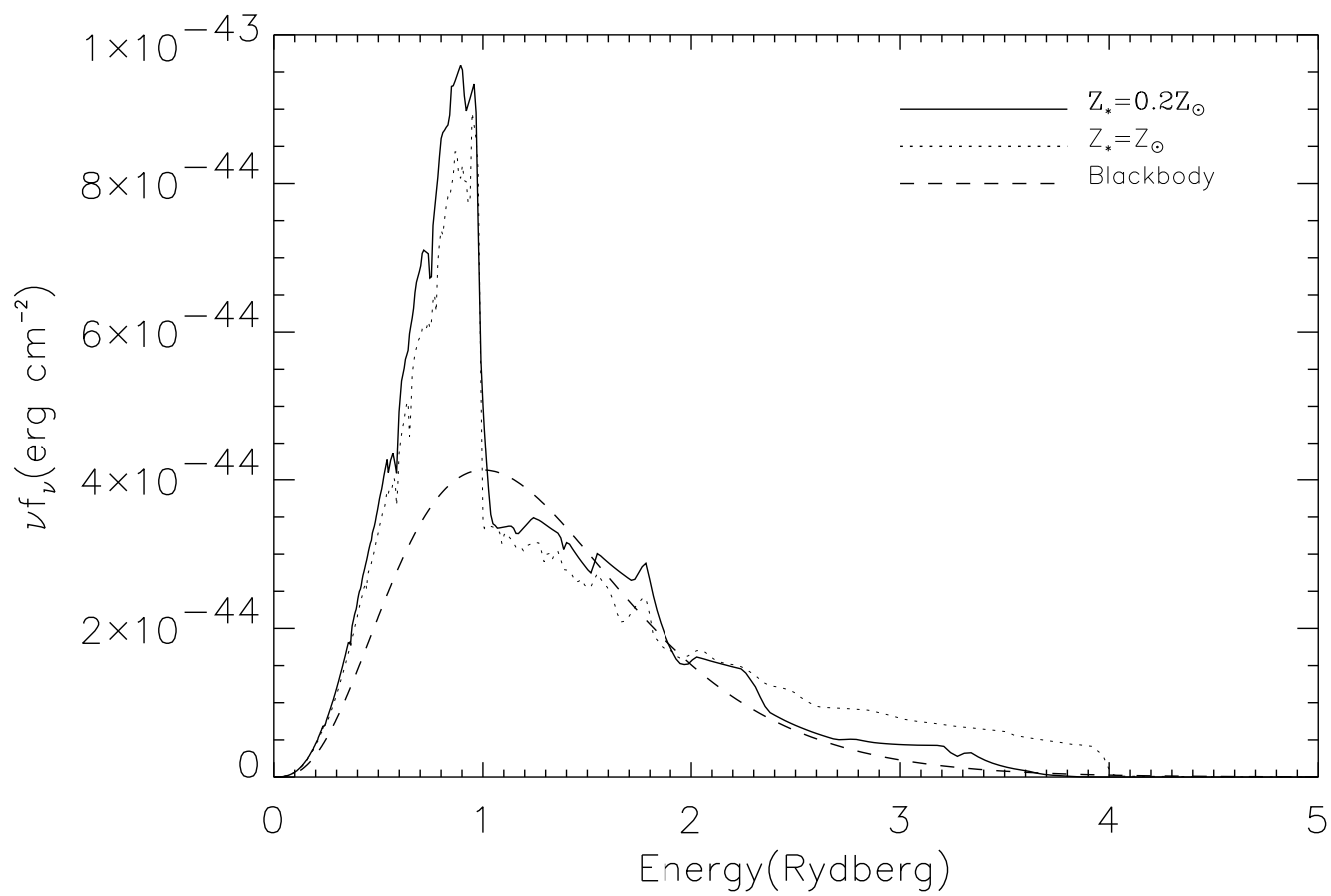


Fig. 1.— Ionizing continuum spectra used in the models. All the spectra are normalized to the same total number of ionizing photons.

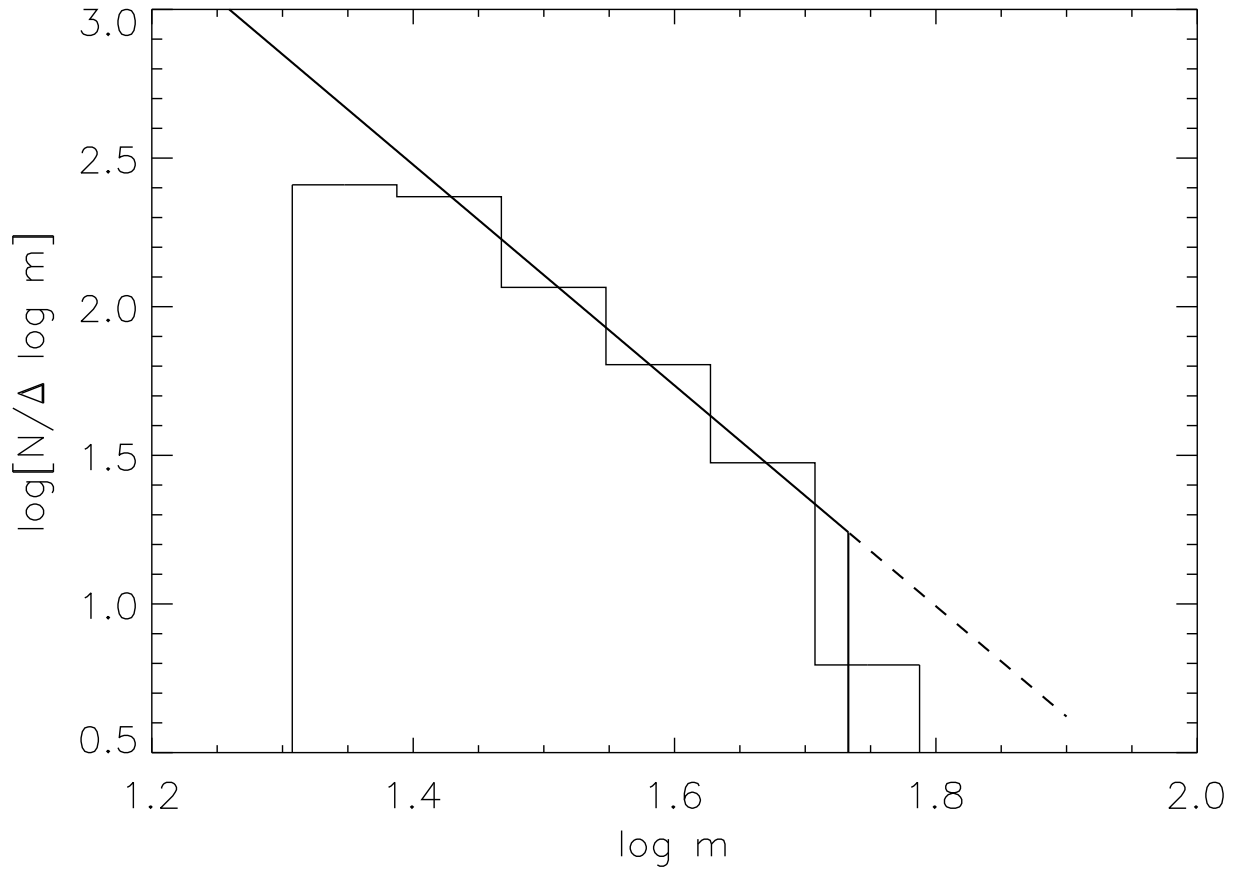


Fig. 2.— IMF derived from Table 1. The straight line represents the IMF derived from the four central bins and it has a slope of  $-3.7 \pm 0.4$ . This IMF has an upper mass cutoff of  $54.1 M_{\odot}$  and it is only representative for masses higher than  $24 M_{\odot}$ .